The Astrophysical Journal, 690:1412–1423, 2009 January 10 doi:10.1088/0004-637X/690/2/1412

A COSMIC-RAY PRECURSOR MODEL FOR A BALMER-DOMINATED SHOCK IN TYCHO'S SUPERNOVA REMNANT

A. Y. Wagner[1,4], J.-J. Lee[2], J. C. Raymond[3], T. W. Hartquist[1], and S. A. E. G. Falle[1]
[1] School of Physics and Astronomy, University of Leeds, Leeds LS3 1NS, UK; ayw@ast.leeds.ac.uk
[2] Department of Astronomy and Astrophysics, Pennsylvania State University, 525 Davey Laboratory, University Park, PA 16802, USA
[3] Harvard-Smithsonian Center for Astrophysics, 60 Garden Street, Cambridge, MA 02138, USA
[4] Current address: Research School of Astronomy and Astrophysics, Mount Stromlo Observatory, Australian National University, Cotter Road, Weston Creek, ACT 2611, Australia
Received 2008 April 21; accepted 2008 September 16; published 2008 December 12

ABSTRACT

We present a time-dependent cosmic-ray (CR) modified shock model for which the calculated Hα emissivity profile agrees well with the Hα flux increase ahead of the Balmer-dominated shock at knot g in Tycho's supernova remnant (SNR), observed by Lee et al. The backreaction of the CR component on the thermal component is treated in the two-fluid approximation, and we include thermal particle injection and energy transfer due to the acoustic instability in the precursor. The transient state of our model that describes the current state of the shock at knot g occurs during the evolution from a thermal gas dominated shock to a smooth CR-dominated shock. Assuming a distance of 2.3 kpc to Tycho's remnant, we obtain values for the CR diffusion coefficient, κ, the injection parameter, ϵ, and the timescale for the energy transfer, τ, of $\kappa = 2 \times 10^{24}\,\mathrm{cm^2\,s^{-1}}$, $\epsilon = 4.2 \times 10^{-3}$, and $\tau = 426\,\mathrm{yr}$, respectively. We have also studied the parameter space for fast ($300\,\mathrm{km\,s^{-1}} \lesssim v_s \lesssim 3000\,\mathrm{km\,s^{-1}}$), time-asymptotically steady shocks and have identified a branch of solutions, for which the temperature in the CR precursor typically reaches 2×10^4 to 6×10^4 K and the bulk acceleration of the flow through the precursor is less than $10\,\mathrm{km\,s^{-1}}$. These solutions fall into the low CR acceleration efficiency regime and are relatively insensitive to shock parameters. This low CR acceleration efficiency branch of solutions may provide a natural explanation for the line broadening of the Hα narrow component observed in nonradiative shocks in many SNRs.

Key words: acceleration of particles – hydrodynamics – line: profiles – methods: numerical – shock waves – supernova remnants

Online-only material: color figures

1. INTRODUCTION

Balmer-dominated filaments in supernova remnants (SNRs) trace fast, nonradiative shocks that propagate into partially neutral, diffuse media. The filaments are sheets of shocked gas seen edge-on (Hester 1987) and have been observed and studied in many SNRs including Tycho's SNR (Chevalier et al. 1980; Kirshner et al. 1987; Smith et al. 1991; Ghavamian et al. 2000, 2001, hereafter G00 and G01, respectively; Lee et al. 2007, hereafter L07), the Cygnus Loop (e.g., Raymond et al. 1983; Hester et al. 1994), RCW86 (e.g., Sollerman et al. 2003), Kepler's SNR (e.g., Blair et al. 1991; Sankrit et al. 2005), SN1006 (e.g., Ghavamian et al. 2002), and four remnants in the Large Magellanic Cloud (LMC; e.g., Smith et al. 1994). This work focuses on modeling a particular Balmer-dominated shock located at knot g in Tycho's SNR (after Kamper & van den Bergh 1978) and recently observed by L07.

The Hα spectral line profile of a Balmer-dominated filament has narrow and broad components, whose widths represent the preshock temperature of neutral H and the postshock temperature of protons, respectively (Chevalier & Raymond 1978). The width of the broad component and the ratio of intensities are diagnostics for the shock speed and the degree of electron–ion temperature equilibration behind the shock. Shock models to quantify these diagnostics were first developed by Chevalier et al. (1980) and later improved by Smith et al. (1991), G01, Heng & McCray (2007), and Heng et al. (2007). Currently, the most advanced nonradiative shock models are those of van Adelsberg et al. (2008). Except for the work by Boulares & Cox (1988), shock models used to interpret optical observations to date have not included modifications of the shock structure due to diffusive shock acceleration (DSA) of cosmic rays (CRs).

Balmer-dominated filaments are usually associated with forward shocks of the expanding SNR bubbles. The only remnant in which Balmer emission from a reverse shock has been observed is SN 1987 (Michael et al. 2003). Forward shocks in SNRs are also sites of CR electron acceleration, as evidenced by synchrotron radio and X-ray emission (Koyama et al. 1995; Gotthelf et al. 2001; Long et al. 2003; Bamba et al. 2005; Cassam-Chenaï et al. 2007), and likely sites of CR ion acceleration (Blandford & Eichler 1987; Drury et al. 2001; Warren et al. 2005). In most cases, Balmer-dominated shocks do not show evidence for synchrotron emission, which suggests that particle acceleration in Balmer-dominated shocks is not efficient. The neutral component in the upstream thermal gas that is required for nonradiative shocks to produce Balmer-dominated filaments may be damping the turbulence necessary for efficient CR acceleration in SNR shocks (Drury et al. 1996). Conversely, the heating of the upstream medium due to efficient CR acceleration may prevent most neutrals from reaching the shock before being ionized (Hester et al. 1994). Two known exceptions where Balmer emission and synchrotron X-ray emission coincide are knot g in Tycho's remnant and a small portion of the eastern rim of SN 1006 (Cassam-Chenaï et al. 2008). However, a direct connection between the Balmer emission producing shock and the X-ray producing shock cannot be made for either case because the X-ray morphology is not resolved to the level of the optical emission and because the effects of projection are uncertain. Many Balmer-dominated filaments are observed to bound regions of X-ray emission whose spectra are consistent with

thermal emission of a shock-heated ambient medium (Hester et al. 1994; Raymond et al. 2007).

The theory of DSA predicts a CR precursor ahead of the gas subshock (Drury & Völk 1981; Berezhko & Ellison 1999), in which the upstream gas is preheated and accelerated over a characteristic distance κ/v_s, where κ is a momentum-averaged CR diffusion coefficient and v_s is the shock speed. The value of κ for CR ions depends on the spectrum of the magnetic wave field, thought to be generated by the CR streaming instability (Bell 1978), and has not been well constrained by observations yet. While in the general ISM $\kappa \sim 3 \times 10^{28}$ to $5 \times 10^{28}\,\mathrm{cm^2\,s^{-1}}$ (Strong et al. 2007), at the forward shocks of SNRs, κ is thought to be close to the Bohm diffusion limit $\kappa_{\mathrm{B}} \approx 3 \times 10^{22}\,\mathrm{cm^2\,s^{-1}}\,(\beta\,B_0/\mu\mathrm{G})^{-1}\left(p/\mathrm{GeV\,c^{-1}}\right)$, where β is the ratio of particle speed to the speed of light, B_0 is the large scale magnetic field, and p is the CR particle momentum (Drury 1983). κ_{B} is the lower limit to κ allowed by the standard theory of DSA, and corresponds to saturated field fluctuations, $\delta B/B_0 = 1$. Sollerman et al. (2003) estimated upper limits for the diffusion coefficient of CR ions in several SNRs in the range $\kappa \sim 10^{25}$ to $2 \times 10^{27}\,\mathrm{cm^2\,s^{-1}}$ from the condition that neutrals must survive ionization while experiencing the amount of heating implied by the Hα narrow component linewidth. The expression derived by Parizot et al. (2006) for the electron diffusion coefficient as a function of the synchrotron X-ray cutoff energy implies that the electron diffusion coefficient for the SNRs studied in their work is within only a factor of a few greater than the Bohm diffusion coefficient.

The spectral shape and the sharply peaked radial profiles of the synchrotron X-ray emission at the forward shocks of young SNRs require a postshock magnetic field strength of the order of $100\,\mu$G (Vink & Laming 2003; Völk et al. 2005; Ballet 2006). Since compression alone is insufficient to produce such a gain in field strength, it is thought that perturbations in the preshock medium generated by the CR streaming instability are nonlinearly amplified beyond $\delta B/B_0 = 1$ (Bell & Lucek 2001; Bell 2004; Parizot et al. 2006). While some simulations show that there exist rapidly growing nonresonant modes (Zirakashvili et al. 2008), these are saturated at $\delta B/B_0 \sim 1$ in other simulations (Niemiec et al. 2008), and the problem of magnetic field amplification in the CR precursor remains unresolved. Another mechanism for wave generation is the CR-driven acoustic instability (Drury 1984; Drury & Falle 1986; Chalov 1988; Kang et al. 1992), which may play a role in prolonging the confinement of high energy CRs in the CR precursor (Berezhko 1986; Malkov & Diamond 2006; Diamond & Malkov 2007).

In general, strong MHD turbulence in the CR precursor leads to energy dissipation by wave damping that will affect the structure of the shock (MacKenzie & Voelk 1982; Caprioli et al. 2008). Although theories of wave damping exist (see e.g., Whang 1997), neither the rate of energy dissipation nor the fractions of the dissipated energy going into internal energy of the various components of the flow (CR electrons and ions, and thermal electrons and ions) is known from observations. In models of DSA, the original treatment of Alfvén wave damping in CR-modified shocks by Völk & McKenzie (1981) is commonly adopted. The damping of acoustic waves, though less common in models of DSA, may also substantially heat the ions (Drury & Falle 1986) or electrons (Ghavamian et al. 2007) of the thermal component.

A further quantity that is important for DSA is the efficiency of injection of particles from the thermal population into the CR population. The fraction of swept-up thermal protons injected into the acceleration process in SNRs is thought to lie in the range 10^{-4}–10^{-2} (Völk et al. 2003; Ellison & Cassam-Chenaï 2005) if particle acceleration is efficient.

If the structure of a nonradiative shock is modified by CRs, several subtle signatures in the optical emission from the shock are expected (Raymond 2001). One signature would be an FWHM of the narrow Hα component broader than $20\,\mathrm{km\,s^{-1}}$, the value expected if there is no CR acceleration for an upstream medium at a temperature of $T_0 \sim 10^4\,\mathrm{K}$. Spectra of many Balmer-dominated filaments associated with shocks over a wide range of Mach numbers show a narrow Hα component with an FWHM in the range 30–$50\,\mathrm{km\,s^{-1}}$ (see Sollerman et al. 2003, Table 1), indicative of some common form of preshock heating. Significant bulk acceleration of the upstream flow through the precursor would also be detectable as a Doppler shift of the narrow component centroid with respect to Hα emission from the upstream gas. With the exception of the filament observed by L07, which also concerns this work, this has not yet been observed. Currently, a CR precursor is the favored mechanism for the inferred preshock heating (Hester et al. 1994; Smith et al. 1994; Sollerman et al. 2003; L07), but no self-consistent model of such a precursor has been compared with data. Here we show that the precursor structures predicted by two-fluid models of CR-modified shocks, including particle injection at the subshock and energy transfer due to the acoustic instability, are consistent with the above features of Hα spectra.

Recently, L07 obtained high-resolution Hα echelle spectra of an optical filament at knot g in Tycho's SNR, covering the postshock region and the ionization precursor far upstream. Knot g, located in the eastern rim ($\alpha = 00^{\mathrm{h}}25^{\mathrm{m}}56\overset{\mathrm{s}}{.}5$, $\delta = 64^\circ09'28''$, J2000.0), is the brightest region in Hα emission in the remnant. The synchrotron X-ray emission is also particularly bright in this region (Decourchelle et al. 2001; Hwang et al. 2002). Radio data and H I absorption studies suggest that the northeastern rim decelerates into an inhomogeneous ambient medium, possibly the edges of a molecular cloud (see Lee et al. 2004, and references therein). The observations by L07 spatially resolved a steep Hα (narrow component) flux increase ahead of the shock discontinuity, distinct from the photoionization precursor (G00), which L07 attributed to enhanced emission from a CR precursor. They also reported a broadening of the narrow component linewidth by $15\,\mathrm{km\,s^{-1}}$ and a redward Doppler shift of the narrow component centroid with respect to that of the distant upstream Hα emission in this region of $5\,\mathrm{km\,s^{-1}}$.

In this paper, we provide a self-consistent CR-modified shock model applied to the observational data from L07. We model the shock structure with a time-dependent hydrodynamic two-fluid code. We adjust model parameters to obtain a best fit for the calculated spatial Hα profile to the observed profile. The two-fluid equations along with the free parameters and boundary conditions of the shock model are described in Section 2. The method of calculation for the Hα emissivity is given in Section 3. A time-dependent transient solution that provides the best fit to the observed spatial Hα profile is presented in Section 4. In Section 5, we discuss the solution space of steady CR-modified shocks, and propose that the branch of solutions for which the CR acceleration efficiency is low may explain the line broadening of the narrow component of the Hα line, observed in many SNRs. We discuss our results in Section 6, and conclude the paper in Section 7.

2. TWO-FLUID THEORY

CR-modified shocks are sometimes studied with the two-fluid description, first developed by Drury & Völk (1981) and Axford

et al. (1982). The CRs are treated as a massless fluid exerting a bulk pressure on the thermal component. The second velocity moment of the CR transport equation provides a conservation equation governing the CR pressure, which is the quantity that directly affects the dynamics of the thermal component. Since we are primarily interested in the backreaction of the CRs on the gas, it is not essential to follow the CR particle distribution in our calculations.

Two-fluid models have been widely implemented in both plane-parallel and spherically symmetric geometry (e.g., Morfill et al. 1984; Boulares & Cox 1988; Jones & Kang 1992; Duffy et al. 1995; Zirakashvili et al. 1996; Fahr et al. 2000). The basic theory has been extended to include, for example, wave dissipation (Völk et al. 1984; Wagner et al. 2007), oblique shocks (Webb et al. 1986; Frank et al. 1995), particle injection (Kang & Jones 1990; Zank et al. 1993; Ko et al. 1997), and radiative cooling (Wagner et al. 2006). The shock structures obtained with the two-fluid theory agree well with those obtained from kinetic theory and with those obtained with Monte Carlo simulations (Kang & Jones 1995, 1997). The computational expense of solving the two-fluid system numerically is far less than that for the latter two methods.

The approximation of the two-fluid theory consists in the limitation that the adiabatic exponent for the CR component, γ_C, cannot be determined self-consistently, and it is, therefore, usually assigned the constant value of 4/3, appropriate for a relativistic gas. In principle, the diffusion coefficient for CRs, κ, is governed by the spectrum of the scattering wavefield, and is thus a function of particle momentum, space, and time. Since two-fluid models lack information about the CR particle spectrum, a momentum-averaged effective diffusion coefficient is commonly used. Although one may prescribe the evolution of the closure parameters, κ and γ_C (e.g., Markiewicz et al. 1990; Jones & Kang 1992; Duffy et al. 1994), we choose to keep them constant as a first step to model the nonradiative shock at knot g.

The main consequence of the backreaction by CRs on the gas is adiabatic heating and compression in the vicinity of the shock discontinuity where the CR pressure gradient is largest. When a substantial fraction of the total energy has gone into CRs, the overall compression ratio exceeds 4 and approaches 7, and the shock discontinuity may be entirely smoothed out, that is, the gas subshock disappears. Such solutions are referred to as "efficient" or "CR dominated." Conversely, if only a small fraction of the shock energy goes into CRs, the solution is termed "inefficient," and the modification of the shock structure is weak.

In the case of fast shocks, such as those responsible for Balmer-dominated filaments in SNRs, some regions of parameter space permit up to three distinct solutions for the same distant upstream conditions and shock parameters. Some of these solutions do not exist as time-asymptotic steady states, but if exactly two solutions exist, one of them is an efficient solution and the other is an inefficient one. It is important to perform time-dependent runs to determine whether a steady solution exists as a time-asymptotic state.

We neglect the dynamics of the wavefield responsible for the scattering of the particles, and thus ignore heating of the gas through Alfvén wave damping. Instead, we invoke source terms that represent the decay of sound waves generated by the acoustic instability (Drury & Falle 1986). We include injection of CR particles at the gas subshock.

In the remaining parts of this section, we first write down the equations for the two-fluid system and the relevant source terms. We then list the free parameters and boundary conditions for our model.

2.1. Equations

The following equations govern the two-fluid medium consisting of the thermal component and the CR component in plane-parallel symmetry:

$$\frac{\partial \rho}{\partial t} + \frac{\partial \rho u}{\partial x} = 0, \tag{1}$$

$$\frac{\partial \rho u}{\partial t} + \frac{\partial \rho u^2}{\partial x} + \frac{\partial P_G}{\partial x} + \frac{\partial P_C}{\partial x} = 0, \tag{2}$$

$$\frac{\partial}{\partial t}\left(\frac{\rho u^2}{2} + \frac{P_G}{\gamma_G - 1}\right) + \frac{\partial}{\partial x}\left(\frac{\rho u^3}{2} + \frac{\gamma_G P_G u}{\gamma_G - 1} + P_C u\right) - P_C \frac{\partial u}{\partial x} = S_G, \tag{3}$$

$$\frac{\partial P_C}{\partial t} + \frac{\partial P_C u}{\partial x} + (\gamma_C - 1) P_C \frac{\partial u}{\partial x} - \kappa \frac{\partial^2 P_C}{\partial x^2} = S_C, \tag{4}$$

where x is the spatial coordinate and t is the temporal coordinate. ρ, P_G, and T denote the mass density, pressure, and temperature of the gas, respectively, and P_C and κ are the CR pressure and the diffusion coefficient, respectively. The two fluids move with bulk velocity u. γ_G, and γ_C are the adiabatic indices for the gas and of the CRs, and are set to the constant values $\gamma_G = 5/3$ and $\gamma_C = 4/3$, respectively. Throughout the paper, subscripts G and C refer to the gas and the CRs and subscripts 0, 1, and 2 denote a distant upstream value, an immediate pre-subshock value, and a postshock value, respectively. Equation (1) expresses mass conservation of the thermal component, and Equation (2) expresses momentum conservation of the thermal component (ρu). Equation (3) governs the total energy density of the thermal component ($(1/2)\rho u^2 + P_G/(\gamma_G - 1)$), and implies that the total energy density of the thermal component is conserved in the absence of CRs. Equation (4) is derived by multiplying the transport equation appropriate for the isotropic part of the CR distribution function by $(4\pi/3)\, p^3\, v$, where v is the CR particle velocity, and integrating that result over all CR particle momenta.

The source terms in Equations (3) and (4) include energy transfer from the CR component to the thermal component due to the acoustic instability in the CR precursor ($S_{C\mathrm{a}}$), as well as CR injection ($S_{C\mathrm{i}}$):

$$S_C = S_{C\mathrm{i}} + S_{C\mathrm{a}}, \tag{5}$$

$$S_G = -\frac{S_C}{\gamma_C - 1}. \tag{6}$$

Both contributions essentially transfer energy from one component to the other, and the total energy of the two-fluid system is always conserved.

The source terms that represent the energy transfer due to the acoustic instability are identical to those used by Wagner et al. (2007):

$$S_{C\mathrm{a}} = \begin{cases} -\frac{\gamma_C - 1}{\gamma_G - 1} P_G \left(\frac{\kappa}{a_G}\left|\frac{\partial P_C}{\partial x}\right| \frac{1}{\gamma_C P_C} - 1\right) \frac{1}{\tau} & \text{if } \frac{\kappa}{a_G}\left|\frac{\partial P_C}{\partial x}\right| \frac{1}{\gamma_C P_C} - 1 > 0\,; \\ 0 & \text{otherwise.} \end{cases} \tag{7}$$

Sound waves are amplified in regions where the relative gradient of the CR pressure, $\gamma_C P_C/|\mathrm{d}P_C/\mathrm{d}x|$, exceeds a critical length scale a_G/κ. Here, $a_G = \sqrt{\gamma_G P_G/\rho}$ is the thermal sound speed. This condition for instability is usually satisfied in the CR precursor because the increase in CR pressure scales as κ/v_s, and $v_s \gg a_G$. The damping of the sound waves leads to a net energy transfer from the CR component to the thermal component. By invoking the source terms (Equation (7)), we bypass the initial perturbations and assume that wave damping occurs at the necessary rate to produce the desired energy transfer. The source term is nonzero if the condition for acoustic instability is satisfied. τ is a time constant that determines the rate of energy transfer, and the term in brackets ensures that the energy transfer drives the flow toward stability.

We may estimate an order of magnitude value for τ from dimensional arguments. If we assume a Kolmogorov-type turbulence spectrum with the largest spatial scale set by the width of the CR precursor, κ/v_s, then the cascade timescale is approximately

$$\frac{\kappa}{v_s v_{\mathrm{A}}} \approx 300\,\mathrm{yr}\left(\frac{\kappa}{10^{24}\,\mathrm{cm^2\,s^{-1}}}\right)\left(\frac{v_s}{1000\,\mathrm{km\,s^{-1}}}\right)^{-1} \times \left(\frac{v_{\mathrm{A}}}{10\,\mathrm{km\,s^{-1}}}\right)^{-1}, \quad (8)$$

where v_{A} is the Alfvén speed. This timescale may be comparable to τ for CR-modified shocks in SNRs.

Jones & Kang (1990; JK90 hereafter), Zank et al. (1993), and Ko et al. (1997) each adopted a different approach to simulate particle injection in two-fluid models. We follow the method employed by JK90, which is a two-fluid version of that employed by Falle & Giddings (1987):

$$S_{C\mathrm{i}} = \frac{1}{2}\,\epsilon\,\rho_1\,u_1\left(\lambda a_{G2}\right)^2 w(x - x_{\mathrm{subshock}}). \quad (9)$$

The source term represents the injection of CR particles with speed λa_{G2} into the immediate postshock flow and the corresponding removal of energy from the thermal component. Following Falle & Giddings (1987) and JK90, we set $\lambda = 2$. The rate at which energy is injected is proportional to the mass flux through the shock and the parameter ϵ determines the strength of injection.

Injection is zero ahead of the subshock and has a Gaussian dependence on distance, w, behind the subshock, which is located at x_{subshock}. The width of the injection zone must be at least 15 cells. It must also be much narrower than κ/v_s in order for the solutions not to be sensitive to the width of the injection region. Following JK90, injection is turned off smoothly but rapidly when the pre-subshock Mach number with respect to $a_{C+G1} = \sqrt{(\gamma_G P_{G1} + \gamma_C P_{C1})/\rho_1}$ is only slightly larger than unity.

Equations (1)–(4) are solved with a second-order finite-difference Godunov scheme on a uniform cell grid. The CR Equation (4) is solved implicitly using a Crank–Nicholson scheme for the diffusion term. The time step is determined by the Courant–Friedrichs condition with the effective sound speed a_{C+G}. The code and technique used are identical to those employed by Wagner et al. (2007).

2.2. Free Parameters

Let $\phi = P_C/P_G$ be the ratio of the CR pressure to the thermal gas pressure. The free parameters of this model are: the shock speed, v_s ($v_s = u_0$ in the shock frame); the ratio of distant upstream CR pressure to distant upstream thermal gas pressure, ϕ_0; the distant upstream number density, n_0, and temperature, T_0; the CR diffusion coefficient, κ; the injection parameter, ϵ; and the timescale of energy transfer due to the acoustic instability, τ. While ϵ, τ, and κ are essentially unconstrained free parameters, we may fix or narrow down the ranges of the other parameters from results of previous observations. All the above named parameters remain constant in time, except for v_s, which changes as the shock structure evolves.

2.3. Boundary and Initial Conditions

For the results presented in this paper, we have assumed a distance of 2.3 kpc to Tycho's SNR. The nonradiative shock at knot g propagates into a photoionization precursor, which is at a temperature of $T_0 \approx 1.2 \times 10^4$ K, and $n_0 \approx 1\,\mathrm{cm^{-3}}$ (G00). The shock speed inferred from previous shock modeling is $(\sim 2000 \pm 200)\,\mathrm{km\,s^{-1}}$ (Chevalier et al. 1980; Smith et al. 1991; G01), although these models have been based on the assumption that the available shock energy is converted solely into thermal energy. The inferred shock speed would be higher if a substantial fraction of the shock energy went into the CR component.

In most environments of the interstellar medium (ISM), the CR pressure is comparable with the thermal gas pressure (Ferrière 1998). We have looked at cases for which $1/3 \leqslant \phi_0 \leqslant 3$. In general, we find that the consequences of increasing or decreasing ϕ_0 on the structure and evolution of a shock were very similar to those of increasing or decreasing ϵ. We, therefore, set $\phi_0 = 1$.

In the case of knot g, there is some uncertainty in the interpretation of the Hα narrow component linewidth, due to the presence of an intermediate width component (G00; L07). G00 and L07 found that an adequate fit to the Hα line profile requires three Gaussian components. The component of intermediate width may be produced by protons undergoing secondary charge exchange or by nonthermal motions. Furthermore, the assumption of Gaussian line profiles may not be appropriate (Raymond et al. 2008). The pre-subshock temperature, T_1, up to which the flow in the CR precursor is heated, is therefore taken to be an unknown quantity prior to modeling. Our shock model for knot g provides an independent estimate of T_1.

L07 estimated the net acceleration of the flow across the precursor, Δu, to be in the range 60–130 km s^{-1}. We require this condition to be met in our shock model.

The initial condition ($t = 0$) for a time-dependent run is an ordinary gas shock, for which $v_s = 2000\,\mathrm{km\,s^{-1}}$, and for which the CR pressure is homogeneous across the grid at the distant upstream value of $\phi_0 = 1$. The time to reach a desired shock structure in any time-dependent run should not exceed the age of the remnant, $t_{\mathrm{SNR}} = 436$ yr.

We employ free-flowing boundary conditions on either side of the grid.

3. Hα PROFILE CALCULATIONS

We assume that the optical radiation from the shock is not coupled to the hydrodynamics of the flow and calculate the emission from the system as a separate step, using the results from the hydrodynamic simulations as boundary conditions. The assumption of separating the radiative processes from the hydrodynamics in the CR precursor is good because the radiative cooling time is of the order of 10^{10} s, while the dynamical timescale across the precursor is of the order of 10^8 s.

In a conventional Balmer-dominated shock, preshock neutral hydrogen atoms swept up by the shock (henceforth, referred to as neutrals) are initially unaffected by the collisionless processes that mediate the shock. Within a short distance behind the shock, the neutrals may be collisionally excited before being ionized, giving rise to a narrow Hα line whose width represents the temperature of the "cold" preshock neutrals. Preshock protons, on the other hand, are instantaneously heated to a postshock temperature given by the Rankine–Hugoniot jump conditions. Charge transfer between the hot postshock protons and cold neutrals entering the shock gives rise to a population of hot postshock neutrals that are responsible for the broad component of the Hα spectral line profile. A significant fraction of Hα emission comes from Lyβ trapping; Lyβ photons from the postshock region are converted to Hα photons through scattering.

However, this conventional picture of a Balmer-dominated shock does not explicitly account for a CR precursor. The existence of a CR precursor can affect the emitted Hα line in a few ways. On the one hand, neutrals are ionized in the precursor and the number of neutrals reaching the shock front is reduced. On the other hand, collisional excitation of neutrals within the precursor serves as an additional source of Hα (and Lyβ) photons. The varying temperature and bulk velocity (and, therefore, density) of the precursor flow will also affect the rate of Lyβ trapping.

We have developed an emission model incorporating the above effects of a CR precursor (J.-J. Lee et al. 2008, in preparation), which is briefly described in the following. We consider a flow consisting of hydrogen and helium. Given a temperature and a velocity profile for the precursor, we calculate the spatial evolution of the ionization states of hydrogen and helium in the precursor and postshock regions. The calculations are essentially identical to those of G01, except that we have explicitly included the effects of the precursor with a given temperature and velocity profiles. We include collisional ionization by electrons and protons. We distinguish between fast and slow neutral hydrogen components, and include charge exchange between neutrals and protons. From the resulting spatial profiles of slow hydrogen atoms and fast hydrogen atoms, we calculate the emissivity of the narrow and broad Hα components. For this, we again include excitation by both electrons and protons. Since a significant fraction of Hα emission comes from Lyβ trapping, we similarly calculate spatial profiles of the Lyβ emissivity and model the radiative transfer of the Lyβ line with a Monte Carlo simulation. The flux of Hα photons arising from the radiative transfer of Lyβ photons is added to the intrinsic Hα flux to give the total Hα emissivity profile.

We apply our emission model to the hydrodynamic model described in Section 2 and compare the results with the observed Hα emissivity profile of L07. For this comparison, the distant upstream H neutral fraction is taken to be 0.85 and He is fully neutral (G00). We assume equal temperatures for the electrons, ions, and neutrals throughout the shock precursor and adopt an equilibration fraction between ion and electron temperatures in the postshock flow of 0.05. We note that results are not very sensitive to the postshock equilibration fraction since excitation by protons in the postshock region is significant for the assumed shock velocity.

4. COMPARISON OF MODEL CALCULATIONS WITH DATA

We have performed a thorough investigation of parameter space for the time-dependent two-fluid system described in Section 2. We find that the observed Hα emissivity requires the flow in the CR precursor to be heated to a pre-subshock temperature of $T_1 = 10^5$ K. However, steady CR-modified shock solutions in the high Mach number regime are of two types. The solutions tend to be either smooth, CR-dominated solutions, or inefficient solutions that are only weakly modified by CRs. In neither branch of solutions are the shock structures very sensitive to the parameters v_s, ϕ_0, κ, τ, and ϵ. As a consequence, we could not find a steady solution in which the gas in the precursor reached a pre-subshock temperature of $T_1 = 10^5$ K and was accelerated by $\Delta u \approx 100\,\mathrm{km\,s^{-1}}$. Blasi et al. (2007) and Caprioli et al. (2008) explored the acceleration timescale and the evolution of the CR acceleration efficiency for SNRs in the Sedov phase, respectively, and they found that the shocks evolve toward a quasi-steady state on a timescale of the order of 10^3 yr. We have, thus, found a transient solution that satisfies the observational constraints. In the following, we first present the shock structure of the transient state and then show its subsequent evolution into a CR-dominated shock.

4.1. Transient State Solution

The transient state occurs during the evolution of a shock that is initially not modified by CRs to a shock that is CR dominated. Figure 1 displays the shock structure of the transient solution for which the calculated Hα emissivity profiles match the observed profiles in the precursor region. In all six panels, the shock profiles are shown in the frame comoving with the shock, and the flow enters the grid from the right.

The location of the gas subshock at $x = 0$ is clear from the sudden increase in the broad component flux. We take this to be the outermost nonradiative shock at knot g or the outermost part of a corrugated shock front (wavy sheet). We are primarily interested in modeling the Hα narrow component flux upstream of the gas subshock. We assume that this emission originates from the upstream gas heated by a CR precursor. The model must also reproduce the immediate postshock narrow and broad component fluxes. The extended emission further downstream is probably due to multiple shock fronts superimposed in the line of sight (LOS). We do not require our model to reproduce the extended emission downstream of the immediate postshock region.

This transient state is reached within 420 yr of the evolution of a shock for which $\kappa = 2 \times 10^{24}\,\mathrm{cm^2\,s^{-1}}$, $\tau = 426$ yr, $\epsilon = 4.2 \times 10^{-3}$. At time $t = 0$, the shock is not modified by CRs, $v_s = 2000\,\mathrm{km\,s^{-1}}$, and $\phi = 1$ throughout the grid. At time $t = 420$ yr (Figure 1), the shock structure is one in which the thermal pressure still dominates and about 10% of the shock energy has gone into CRs. The bottom two panels show that the narrow and broad Hα emissivity profiles match the observed profiles.

The very close similarity between the values of τ and t_{SNR} is coincidental, although it does reassure us that the value for τ is physically reasonable. The value of τ is also consistent with the estimate of the timescale from dimensional arguments given in Section 2.1.

The parameters κ, τ, and ϵ affect the degree of agreement of the calculated Hα emissivity profile with the observed Hα profile in different ways. The spatial extent of the observed Hα emission fixes the value of κ at $2 \times 10^{24}\,\mathrm{cm^2\,s^{-1}}$. For a given value of κ, we find that τ primarily governs the balance between heating and deceleration of the gas in the shock precursor during the evolution of the shock, while ϵ primarily determines the rate at which the CR acceleration (and shock modification) takes place.

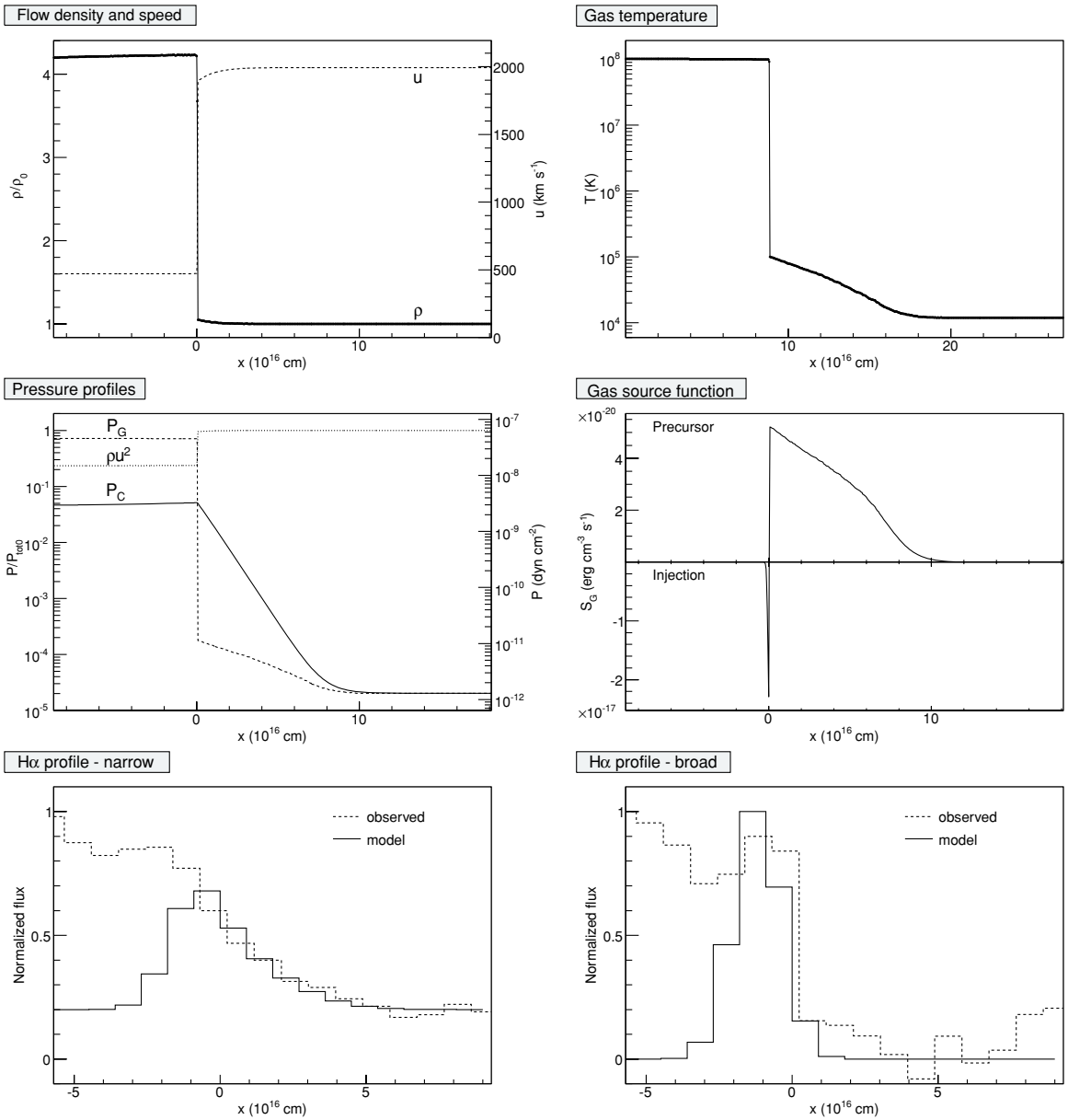

Figure 1. Shock structure of the transient solution for which the calculated Hα emissivity profiles match the observed profiles. The gas subshock is located at $x = 0$. The transient state is reached at time $t = 420$ yr during the evolution of a shock, which was initially ($t = 0$) not modified by CRs (see Figure 3). The shock parameters are $v_s = 2000\,\mathrm{km\,s^{-1}}$, $\phi_0 = 1$, $\kappa = 2 \times 10^{24}\,\mathrm{cm^2\,s^{-1}}$, $\tau = 426$ yr, and $\epsilon = 4.2 \times 10^{-3}$. The shock profiles are shown in the shock frame. The upper part of the panel displaying the source functions is the energy transfer due to the acoustic instability. The lower part of that panel shows the energy transfer due to injection. The model Hα profile is slightly offset along x from the observed Hα profile for visual clarity.

Figure 2 shows the temperature and velocity structure of the CR precursor for several shocks that do not include injection ($\epsilon = 0$). The model for which the values of all parameters other than ϵ are identical to those of the model shown in Figure 1 does not evolve into a CR-dominated shock. The pre-subshock temperature of the low CR acceleration efficiency steady solution is $T_1 = 3.4 \times 10^4$ K and $\Delta u < 1\,\mathrm{km\,s^{-1}}$. The calculated H$\alpha$ narrow component profile of this model does not reproduce the observed profile. We find that a lower value of τ results in neither a larger value of T_1 nor a better fit to the data. In the absence of injection, the lowest value of τ for which the solution evolves into a CR-dominated solution is $\tau \approx 698$ yr. The preshock heating for this shock, as it evolves toward a CR-dominated state, is larger than in the case of shocks for which $\tau > 698$ yr. However, at $t = 420$ yr, this model does not describe the observed Hα either. An alternative to invoking injection in order to decrease the acceleration timescale is to chose a smaller diffusion coefficient. To obtain a shock structure at $t = 420$ yr for which $T_1 = 10^5$ K and $\Delta u = 100\,\mathrm{km\,s^{-1}}$ requires $v_s = 2200\,\mathrm{km\,s^{-1}}$, $\kappa = 10^{23}\,\mathrm{cm^2\,s^{-1}}$, and $\tau = 412$ yr. The calculated Hα profile for this shock model also fails to explain the observed profile. The model Hα profiles in Figure 2 are very similar, due to the coarse binning and the fact that the emission is dominated by photons from Lyβ trapping. The disagreements between the data and the results of the models without injection lead us to conclude that injection is a necessary ingredient in a shock model that adequately describes the emission from knot g.

The shock structure shown in Figure 1 can, in fact, be reached at an earlier time by increasing the value of the injection parameter, ϵ. τ need only be somewhat reduced, and κ remains unchanged. For example, the evolution of a shock that is initially

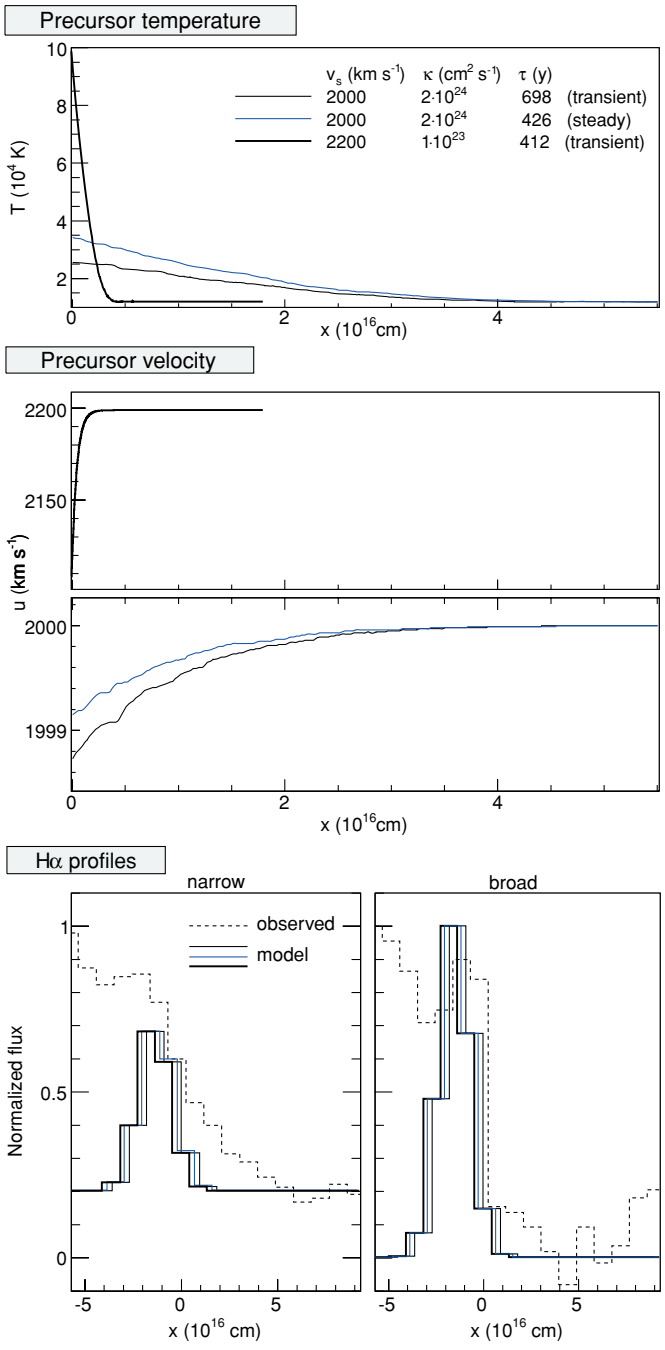

Figure 2. Precursor temperature, velocity, and observed and model Hα profiles of shocks that do not include injection. The different values for v_s, τ and κ are indicated. The normalization for the Hα emissivity profiles is arbitrary and separate for the narrow and broad component profiles. The model profiles are slightly offset along x with respect to each other and the observed profile for clarity. The model Hα profiles are very similar, due to the coarse binning and the fact that the emission is dominated by photons from Lyβ trapping. None of the shock models without injection give a satisfactory fit to the Hα emissivity data (particularly the narrow component). We conclude that injection is necessary in a model that can explain the data.

(A color version of this figure is available in the online journal.)

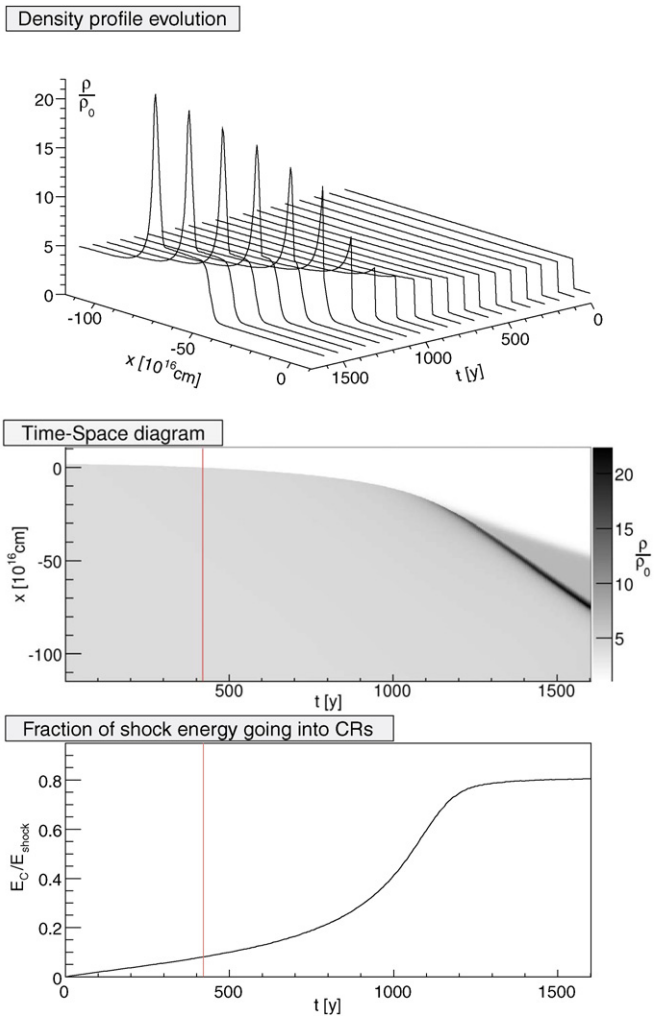

Figure 3. Evolution of a shock, which was initially not modified by CRs, and for which $v_s = 2000\,\mathrm{km\,s^{-1}}$, $\phi_0 = 1$, $\kappa = 2 \times 10^{24}\,\mathrm{cm^2\,s^{-1}}$, $\tau = 426\,\mathrm{yr}$, $\epsilon = 4.2 \times 10^{-3}$. The transient state shown in Figure 1 occurs during a phase in which the thermal pressure dominates. During the rapid transition to a CR dominated, smooth shock, beginning at $t \sim 1000\,\mathrm{yr}$, a density spike forms (see Figure 4). All profiles are shown in the frame comoving with the shock at $t = 0$. The time–space diagram shows the same results as the sequence of profiles. The flow enters the grid from the top. The vertical line in the time–space diagram and in the panel showing the fraction of shock energy going into CRs as a function of time marks the instant in time the transient state occurs ($t = 420\,\mathrm{yr}$).

(A color version of this figure is available in the online journal.)

not modified by CRs at $t = 0$ will pass through a transient state very similar to that shown in Figure 1 at $t = 220\,\mathrm{yr}$ if $\epsilon = 8.0 \times 10^{-3}$, $\tau = 422\,\mathrm{yr}$ and $\kappa = 2 \times 10^{24}\,\mathrm{cm^2\,s^{-1}}$. The condition that the time at which the transient state is reached must be less than t_{SNR} implies that $\epsilon \approx 4.2 \times 10^{-3}$ is a lower limit for the injection parameter. The transient state cannot be reached with a model in which the only CRs are those swept up by the shock (i.e., $\epsilon = 0$), even if $\phi_0 = 3$.

4.2. Time Evolution of a Model

In Figure 3, we show the entire time evolution of a shock that acquires the transient state presented in Section 4.1 at time $t = 420\,\mathrm{yr}$. The fractional gain in CR pressure initially proceeds approximately linearly in time, and the transient state at $t = 420\,\mathrm{yr}$ occurs during a phase of evolution in which the shock modification is still relatively weak. The transition from a weakly CR-modified shock that contains a gas subshock to a smooth CR-dominated shock is quite rapid. The shock speed recedes to $v_s \approx 1830\,\mathrm{km\,s^{-1}}$. During this phase, a density "spike" develops due to a temporary overcompression arising from the combined compression across the CR precursor and the gas subshock. Within a region of width comparable to the diffusion length scale, the density is enhanced by a factor greater than 20

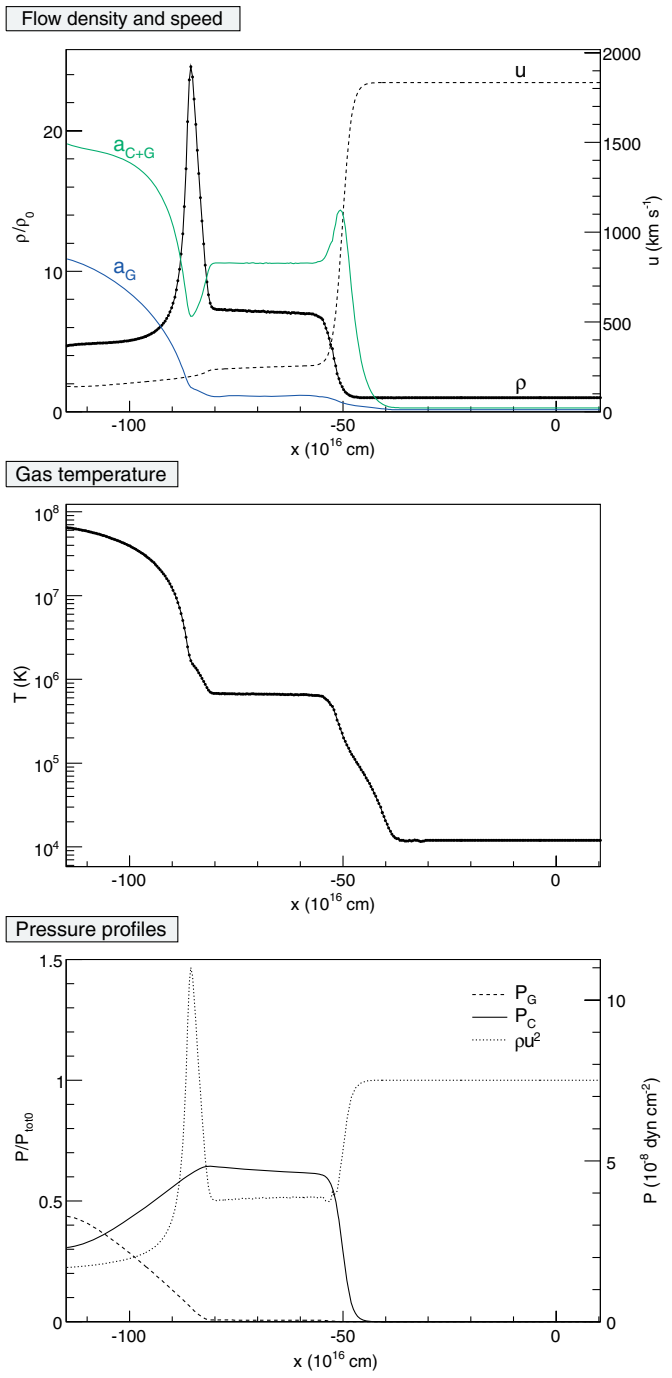

Figure 4. Shock structure at time $t = 1600$ yr in the evolution of the model shown in Figure 3. A density spike has formed during the rapid transition to a CR-dominated shock and is now traveling downstream. The flow upstream of the density spike is supersonic with respect to a_G, but subsonic with respect to a_{C+G}, while the flow downstream of the spike is subsonic with respect to a_G. The density spike may be long-lived and may play a role in the enhancement of the magnetic field downstream and affect the morphology of synchrotron emission from shocks that accelerate CRs.

(A color version of this figure is available in the online journal.)

with respect to the distant upstream density, and a factor of 3 with respect to the density in the immediate postshock region. The density spike travels downstream at approximately 210 km s^{-1} with respect to the smooth CR-dominated shock. In Figure 4, we show the density, velocity, temperature, and pressure structure of the shock after it has developed into a CR-dominated shock ($t = 1600$ yr in the evolution shown in Figure 3).

The density spike in time-dependent CR-modified shocks was first noticed by Dorfi (1984), and its formation was explained by Drury (1987) and JK90. The portion of the postshock flow in which the CR pressure dominates is bounded by the forward shock and the density spike. The flow upstream of the density spike is supersonic with respect to a_G but subsonic with respect to a_{C+G}, and the flow downstream of the density spike is subsonic with respect to a_G. The density spike may, therefore, be long-lived as it moves downstream, although Jun & Jones (1997) demonstrated that the flow through the density spike forms Rayleigh–Taylor instabilities that reduce the density enhancements slightly. Its formation certainly warrants attention in spherically symmetric or three-dimensional simulations of SNR blast waves, as it may play a role in the enhancement of magnetic fields and the morphology of synchrotron emission (Cassam-Chenaï et al. 2007).

A factor of 2–4 enhancement in the thermal X-ray brightness with respect to the local average may be a signature for a density spike traveling downstream of a strongly CR-modified shock. This feature would probably be difficult to detect due to projection effects, contamination from ejecta clumping near the forward shock, and low temperatures of the thermal component (see Figure 4).

5. WEAKLY CR-MODIFIED STEADY SHOCKS AND THE Hα LINEWIDTH OF BALMER-DOMINATED FILAMENTS

The solution space of two-fluid models for steady, high Mach-number ($M \gtrsim 30$), adiabatic, CR-modified shocks contains solutions of high CR acceleration efficiency (i.e., $\phi_2 \gtrsim 1$) and low CR acceleration efficiency (i.e., $\phi_2 \ll 1$). For some combination of shock parameters and distant upstream conditions, there exist multiple solutions. Becker & Kazanas (2001) derived exact analytic expressions for the domains in solution space that contain multiple solutions and the domains in which the solutions exhibit a gas subshock. Malkov et al. (2000) investigated the conditions under which such a bifurcated system may self-regulate.

If $S_G = S_C = 0$ and if ϕ_0 is less than some critical value ϕ_c that depends on the shock Mach number, then for any given distant upstream state, there are three possible postshock states. Of the three solutions, the one for which the CR acceleration efficiency is intermediate, is unstable (Mond & Drury 1998), and does not exist as a time-asymptotic state (Donohue et al. 1994). The solution for which CR acceleration is most efficient exists if (and only if) it is smooth, that is, it does not contain a gas subshock.

Finite source terms determine whether a shock that accelerates CRs evolves into a CR-dominated shock or a shock for which ϕ_2 remains small. For high Mach-number shocks $\phi_c \ll 1$ if $S_G = S_C = 0$. In this case, the solutions bifurcate only if the distant upstream CR pressure is low compared to the pressure of the thermal component, and steady solutions are mostly CR-dominated shocks. However, if $S_{Ca} < 0$, we find that ϕ_c approaches unity, that is, the solution space is bifurcated if the distant upstream CR pressure is comparable to the thermal gas pressure. This gives rise to the existence of the low CR acceleration efficiency branch in high Mach-number shocks for which $\phi_0 \sim \phi_c \sim 1$.

In Figure 5, we show the structure of a shock for which $v_s = 2000$ km s^{-1}, $\kappa = 2 \times 10^{24}$ cm^2 s^{-1}, $\phi_0 = 1$, $\tau = 634$ yr, and $\epsilon = 1.0 \times 10^{-5}$. The pair of values for τ and ϵ lies near the upper boundary of values beyond which a low CR acceleration efficiency solution does not exist (see the Appendix). The

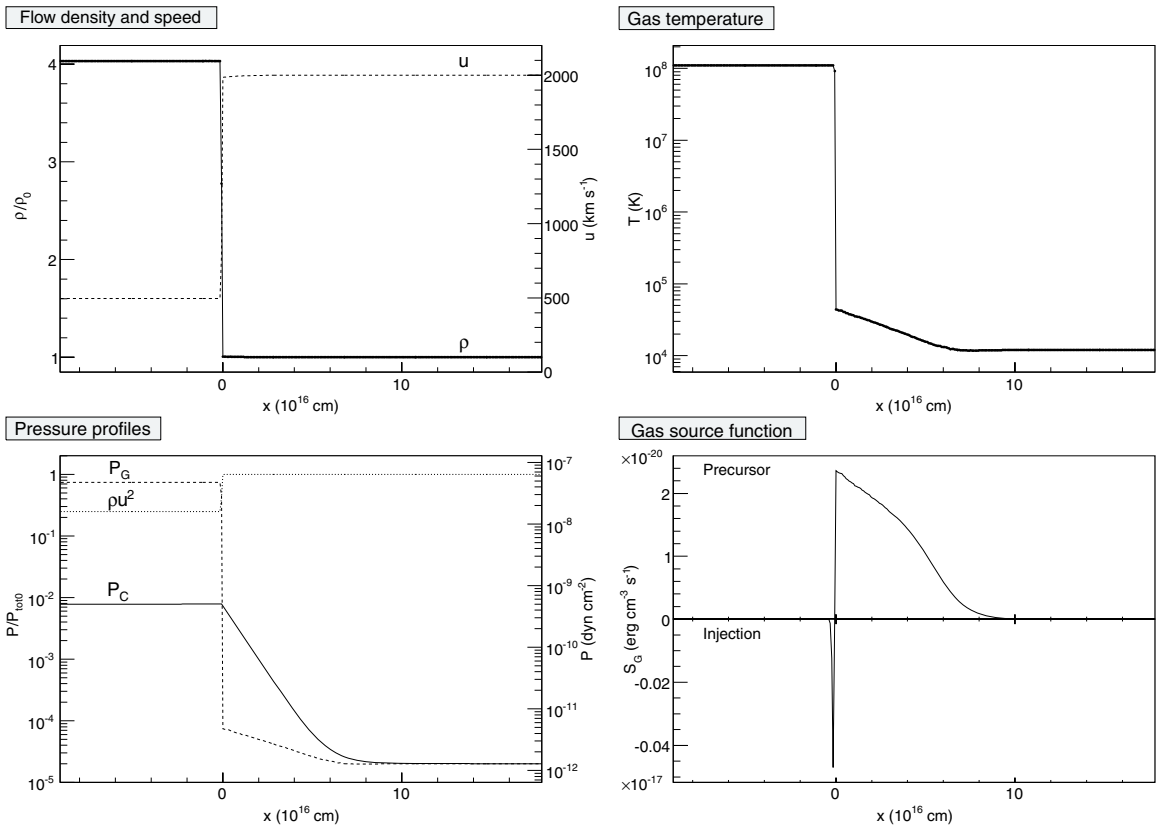

Figure 5. Profiles of a steady shock in the low CR acceleration efficiency branch of solutions. $v_s = 2000\,\mathrm{km\,s^{-1}}$, $\kappa = 2 \times 10^{24}\,\mathrm{cm^2\,s^{-1}}$, $\phi_0 = 1$, $\tau = 634\,\mathrm{yr}$, and $\epsilon = 1.0 \times 10^{-5}$. The gas subshock is located at $x = 0$, and the profiles are shown in the frame of the shock. The upper part of the panel displaying the source functions is the energy transfer due to the acoustic instability. The lower part of that panel shows the energy transfer due to injection. The set of values for τ and ϵ yield the maximum bulk acceleration of the flow through the CR precursor, $\Delta u \approx 10\,\mathrm{km\,s^{-1}}$. The temperature in the precursor reaches $T_1 = 4.2 \times 10^4\,\mathrm{K}$ immediately ahead of the gas subshock. Most solutions in the low CR acceleration efficiency branch are shocks structures similar to the above.

pre-subshock temperature reaches $T_1 = 4.2 \times 10^4\,\mathrm{K}$ and the net acceleration across the precursor is $\Delta u = 10\,\mathrm{km\,s^{-1}}$.

The shock structures in the low CR acceleration efficiency branch of steady solutions do not vary much with shock speed in the range $300\,\mathrm{km\,s^{-1}} \lesssim v_s \lesssim 3000\,\mathrm{km\,s^{-1}}$, which we have explored. We find that in these shocks, no more than 1% of the shock energy is channeled into the CR component. The choice of $\tau = 634\,\mathrm{yr}$ and $\epsilon = 1.0 \times 10^{-5}$ (Figure 5) yields the largest value for Δu that is possible for a steady shock in the low CR acceleration efficiency branch of solutions, for which $v_s = 2000\,\mathrm{km\,s^{-1}}$, $\kappa = 2 \times 10^{24}\,\mathrm{cm^2\,s^{-1}}$, and $\phi_0 = 1$.

For very small values of τ and large values of ϵ, we find solutions in which the pre-subshock temperature exceeds $10^5\,\mathrm{K}$ and $\Delta u \to 0$. In the greater part of parameter space, however, including cases for which $\epsilon = 0$, the preshock temperature reaches 2–6 $\times 10^4\,\mathrm{K}$, and $\Delta u = 0$–$10\,\mathrm{km\,s^{-1}}$. We also note that the steady solutions of the low CR acceleration efficiency branch are reached very quickly, usually within $t < 100\,\mathrm{yr}$, if the initial conditions at $t = 0$ are those of a shock that is not modified by CRs.

The insensitive nature of the low CR acceleration efficiency branch of steady solutions to τ, ϵ, and v_s, provided that they do not exceed critical values for low CR acceleration efficiency steady solutions to exist, may be an explanation for the small range of FWHM (30–50 $\mathrm{km\,s^{-1}}$) for the narrow component of the Hα line observed in Balmer-dominated filaments of many SNRs (Sollerman et al. 2003). Currently, other models of nonradiative shocks, which do not include CRs, are not able to predict the FWHM of 30–50 $\mathrm{km\,s^{-1}}$. Furthermore, the lack of observed bulk Doppler shift in the narrow component is also consistent with the small values for Δu that we obtain. Since only a small fraction of the shock energy goes into the CR component, the shock speeds inferred from previous models applied to nonradiative shocks in SNRs remain valid.

6. DISCUSSION

The results from the time-dependent solutions presented in Section 4 depend on the assumed distance to Tycho's SNR. The canonical value, also assumed here, is $d = 2.3\,\mathrm{kpc}$. Lee et al. (2004) briefly reviewed the debate on the distance to Tycho's SNR. While most authors adopt $d = 2.3\,\mathrm{kpc}$ as established by Chevalier et al. (1980) and subsequently confirmed by several other studies (see Strom 1988), Schwarz et al. (1995) argued for a value of $4.6 \pm 0.5\,\mathrm{kpc}$, based on 21 cm absorption features. However, Black & Raymond (1984) found that absorption features at those velocities were present in the spectra of stars within 2.5 kpc that were close to Tycho on the sky. The calculations by Völk et al. (2007) together with the high energy γ-ray flux upper limit from *HEGRA* (Aharonian et al. 2001) implied a distance $4\,\mathrm{kpc} \gtrsim d \gtrsim 3.3\,\mathrm{kpc}$. If the distance to the remnant is greater than 2.3 kpc, then the shock speed inferred from proper motions and the intrinsic width of the CR precursor would be larger. The values for κ and τ must be scaled accordingly to obtain a model whose calculated spatial Hα emissivity profile matches the observed profile. ϵ must also be increased to allow for the desired transient state to be reached

within $t < t_{\rm SNR}$. However, van Adelsberg et al. (2008) applied their improved shock models to the Hα data and obtained a 15% slower shock speed of $v_s = 1600$–$1700\,{\rm km\,s^{-1}}$ under the assumption that $P_C/P_G = 0$. The slower shock speed would lead to a correspondingly smaller distance to Tycho's SNR. Our result that $\sim$10% of the shock energy goes into CRs during the current state of the shock at knot g would imply a 5% increase in v_s, partially compensating for the lower shock speed inferred by van Adelsberg et al. (2008).

Although the spatial emissivity profile of the Hα narrow component places a stringent constraint on κ, a separate upper limit for the width of the CR precursor comes from the fact that a substantial fraction of hydrogen atoms must avoid ionization ahead of the gas subshock in order to produce the observed broad component. Thus, it is important that our model describes the narrow component flux from the CR precursor and the immediate postshock broad to narrow component flux ratio. For the values of the diffusion coefficient, distant upstream density, and required preshock temperatures in this problem, the CR precursor length scale is much shorter than the preshock electron, proton, and photon ionization length scales, and the H ionization fraction remains nearly constant throughout the CR precursor. This justifies our choice to adopt the distant upstream neutral fraction of 85% derived from the photoionization model by G00 as a fixed boundary condition. A different choice of upstream ionization fraction would affect the immediate postshock ratio of broad to narrow component fluxes, as well as the rate of Lyβ trapping in the CR precursor and, therefore, the spatial Hα profile in front of the gas subshock. The upstream density n_0 only plays a small role in determining the Hα narrow component flux from the CR precursor through enhancing Lyβ trapping in the precursor region close to the gas subshock. The more significant property that determines the spatial flux profiles is the shock temperature profile, in particular the value of the pre-subshock temperature.

The pre-subshock temperature $T_1 = 10^5$ K inferred from our model is larger than the temperature of $\sim 4 \times 10^4$ K implied by the narrow component linewidth in the data of L07. A possible reason for this is the single-temperature approximation we use for the precursor gas. The neutrals may have a lower temperature if the length scale for charge exchange is a significant fraction of the CR precursor length scale. This may be the case for shocks propagating at speeds $v_s \gtrsim 2000\,{\rm km\,s^{-1}}$ into a medium of low fractional ionization.

It should be noted that the calculated Hα emissivity is sensitive to the ratio of electron-to-ion temperatures in the CR precursor. We have adopted a ratio of unity, with the assumption that some plasma-physical process provides the requisite electron heating throughout the CR precursor. Possible processes include the resonant exchange of energy between electrons and protons via lower hybrid waves excited, for example, by the two-stream instability due to shock-reflected ions (Laming 2001) or by the same mechanism that induces high-frequency magnetosonic waves (Ghavamian et al. 2007).

In the mechanism for wave dissipation proposed by Ghavamian et al. (2007), the electrons may attain a temperature of up to 0.3 keV in a CR precursor. For a shock for which $v_s = 2000\,{\rm km\,s^{-1}}$ and the preshock density is $n_0 = 1\,{\rm cm^{-3}}$, this would imply a precursor width of less than $\sim 10^{16}$ cm to avoid complete ionization of the neutrals. This is smaller than the precursor width observed in knot g, suggesting that the electron temperature is considerably lower.

Based on a study of the Tycho remnant's X-ray morphology and spectral characteristics, Warren et al. (2005) proposed that the forward shock at most azimuthal angles is strongly CR modified. A shock compression ratio approaching 7 could explain the proximity between contact discontinuity and forward shock, though projection effects may allow a smaller compression ratio (Cassam-Chenaï et al. 2008). Knot g is situated at an azimuthal angle approximately 80° east of north, and is clearly recognizable as a local minimum in the ratio of the radius of the contact discontinuity to that of the forward shock (Figure 4 of Warren et al. 2005). Assuming that the X-ray shock and the Balmer-dominated shock at knot g are directly associated, the small ratio of radii in the direction of knot g is consistent with our shock model in the transient state: the shock in the transient state is still in the phase in which the shock modification due to CRs is relatively weak, although it develops into a CR-dominated shock.

Although the evolution of the shock in our time-dependent run into a CR-dominated state (Section 4.2) is physical within the framework of the two-fluid theory (Section 2), the question of whether it is a realistic description of the subsequent evolution of the Balmer-dominated shock at knot g must be approached with care. Our plane-parallel model accounts neither for adiabatic losses due to expansions perpendicular to the shock normal nor for particle escape upstream. These two effects may appreciably reduce the CR acceleration efficiency. For example, the steady-state, kinetic shock models of Caprioli et al. (2008) that include particle escape, and the spherically symmetric, kinetic models of Kang & Jones (2006) predict that the acceleration efficiency, which they defined as $P_{C2}/\rho_0 u_0$, reaches 60% during the Sedov phase, whereas we obtain an equivalent efficiency greater than 70% in our time-dependent run. The absence of losses in our model should not significantly affect the early phase of the evolution during which CR modification is still weak, and during which the transient state that describes the Balmer-dominated shock at knot g occurs.

The shock models presented in this work are based on the interpretation of the observations by L07 that the steep rise in the flux of the Hα narrow component ahead of the shock front is due to a CR precursor. The possibility of other types of precursors remains. Of these, a fast neutral precursor is currently thought to be the most likely alternative candidate. A fast neutral precursor is mediated by the hot postshock neutrals (those responsible for the broad component of the Hα line), which escape upstream and deposit some energy via charge exchange and elastic collisions. The calculations by Lim & Raga (1995) and Korreck (2005), however, predicted that the net heating due to a fast neutral precursor is too small to account for the observed narrow component line broadening. In contrast to a CR precursor, the efficiency of preshock heating by fast neutrals is sensitive to the degree of thermal equilibration between electrons and ions, the shock speed, and the neutral fraction upstream. It is, therefore, difficult to explain the narrow range in line broadening seen in many Balmer-dominated filaments in which diverse shock conditions are obtained.

The possibility that the narrow component flux increase ahead of the gas subshock is due to a superposition of multiple shocks in the LOS has not been ruled out. However, as L07 have argued, a superposition of shocks would imply a gradual flux increase of the broad component ahead of the gas subshock in the same manner as the flux of the narrow component. This is not observed.

7. CONCLUSIONS

In summary, CR acceleration in the forward shocks of SNRs results in the heating and acceleration of the preshock medium, which may explain some features of the optical emission of Balmer-dominated filaments. We have found a transient state in the evolution of a shock from one that is initially not modified by CRs to one that is CR dominated, for which the calculated Hα emissivity profile matches the emissivity profile across the Balmer-dominated filament in knot g observed by Lee et al. (2007). The values of the parameters for this shock model are an initial shock speed $v_s = 2000\,\mathrm{km\,s^{-1}}$, a distant upstream CR pressure to thermal gas pressure ratio $\phi_0 = 1$, a diffusion coefficient $\kappa = 2 \times 10^{24}\,\mathrm{cm^2\,s^{-1}}$, an energy transfer timescale due to the acoustic instability $\tau = 426\,\mathrm{yr}$, and a lower limit to the injection parameter $\epsilon = 4.2 \times 10^{-3}$.

The structure of steady shocks that belong to the low CR acceleration efficiency branch of solutions for fast shocks is relatively insensitive to the values of τ, ϵ, κ, and v_s in the range $300\,\mathrm{km\,s^{-1}} < v_s < 3000\,\mathrm{km\,s^{-1}}$, provided that the parameters are chosen such that a steady solution in the low CR acceleration efficiency branch exists. The solutions are usually reached as time-asymptotic states within less than 100 yr, even if $\epsilon = 0$. The mild heating of the preshock gas up to typically $2\text{–}6 \times 10^4$ K and the negligible bulk acceleration of the flow in the precursor ($\Delta u \leqslant 10\,\mathrm{km\,s^{-1}}$) may provide a natural explanation for the characteristic broadening of the narrow component linewidth that is observed to lie in the small range FWHM = 30–50 $\mathrm{km\,s^{-1}}$ in many SNRs, and the lack of bulk Doppler shift of the narrow component observed for these cases.

The authors thank the referee for carefully reviewing the manuscript and providing feedback that has led to a substantial improvement of the paper. A.Y.W is grateful for financial support from the Smithsonian Institution Scholarly Studies Fund, and the hospitality during the course of this work at the CfA. This work was funded by the *HST* grant number GO-10577 to the Smithsonian Institution.

APPENDIX

In the following, we give an example of the limits for τ and ϵ within which the low acceleration efficiency branch of steady CR-modified shocks, as described in Section 5, exist.

If $\epsilon = 0$, the exact value for ϕ_c depends only on the dimensionless quantity $\eta = \tau v_s^2/\kappa$. The method to find the range in η for which two distinct solutions exist for a given distant upstream state is described in Wagner et al. (2007) for radiative shocks of a lower Mach number. Here, we find, for example, that for shocks for which $v_s = 2000\,\mathrm{km\,s^{-1}}$, $\phi_0 = 1$, $\kappa = 2 \times 10^{24}\,\mathrm{cm^2\,s^{-1}}$, and $\epsilon = 0$, the low CR acceleration efficiency branch of solutions exists up to $\tau_a \approx 634$ yr, and the (smooth) high CR acceleration efficiency branch of solutions exists down to $\tau_b \approx 63$ yr. In the range $\tau_b < \tau < \tau_a$, both an inefficient and an efficient steady solutions are allowed.

As expected, a large injection parameter drives the solution toward the one that is CR dominated. For example, if $v_s = 2000\,\mathrm{km\,s^{-1}}$, $\kappa = 2 \times 10^{24}\,\mathrm{cm^2\,s^{-1}}$, $\phi_0 = 1$, and $\tau = 426$ yr, the critical value for ϵ above which a low CR acceleration efficiency solution cannot exist is $\sim 1.0 \times 10^{-4}$. Conversely, a shock for which v_s, κ, ϕ_0 are the same as above but $\epsilon = 4.2 \times 10^{-3}$ (the value obtained from the model in Section 4) can only remain in the inefficient branch of solutions if $\tau \lesssim 63$.

REFERENCES

Aharonian, F. A., et al. 2001, A&A, 373, 292
Axford, W. I., Leer, E., & McKenzie, J. F. 1982, A&A, 111, 317
Ballet, J. 2006, Adv. Space Res., 37, 1902
Bamba, A., Yamazaki, R., Yoshida, T., Terasawa, T., & Koyama, K. 2005, ApJ, 621, 793
Becker, P. A., & Kazanas, D. 2001, ApJ, 546, 429
Bell, A. R. 1978, MNRAS, 182, 147
Bell, A. R. 2004, MNRAS, 353, 550
Bell, A. R., & Lucek, S. G. 2001, MNRAS, 321, 433
Berezhko, E. G. 1986, Sov. Astron. Lett., 12, 352
Berezhko, E. G., & Ellison, D. C. 1999, ApJ, 526, 385
Black, J. H., & Raymond, J. C. 1984, AJ, 89, 411
Blair, W. P., Long, K. S., & Vancura, O. 1991, ApJ, 366, 484
Blandford, R., & Eichler, D. 1987, Phys. Rep., 154, 1
Blasi, P., Amato, E., & Caprioli, D. 2007, MNRAS, 375, 1471
Boulares, A., & Cox, D. P. 1988, ApJ, 333, 198
Caprioli, D., Blasi, P., & Amato, E. 2008, arXiv:0807.4259
Caprioli, D., Blasi, P., Amato, E., & Vietri, M. 2008, ApJ, 679, L139
Cassam-Chenaï, G., Hughes, J. P., Ballet, J., & Decourchelle, A. 2007, ApJ, 665, 315
Cassam-Chenaï, G., Hughes, J. P., Reynoso, E. M., Badenes, C., & Moffett, D. 2008, ApJ, 680, 1180
Chalov, S. V. 1988, Sov. Astron. Lett., 14, 114
Chevalier, R. A., Kirshner, R. P., & Raymond, J. C. 1980, ApJ, 235, 186
Chevalier, R. A., & Raymond, J. C. 1978, ApJ, 225, L27
Decourchelle, A., et al. 2001, A&A, 365, L218
Diamond, P. H., & Malkov, M. A. 2007, ApJ, 654, 252
Donohue, D. J., Zank, G. P., & Webb, G. M. 1994, ApJ, 424, 263
Dorfi, E. 1984, Adv. Space Res., 4, 205
Drury, L. O. 1983, Rep. Prog. Phys., 46, 973
Drury, L. O. 1984, Adv. Space Res., 4, 185
Drury, L. O. 1987, in Sixth International Solar Wind Conference, ed. V. J. Pizzo, T. Holzer, & D. G. Sime, (Novosibirsk: Nauka), 521
Drury, L. O., et al. 2001, Space Sci. Rev., 99, 329
Drury, L. O., Duffy, P., & Kirk, J. G. 1996, A&A, 309, 1002
Drury, L. O., & Falle, S. A. E. G. 1986, MNRAS, 223, 353
Drury, L. O., & Völk, H. J. 1981, ApJ, 248, 344
Duffy, P., Ball, L., & Kirk, J. G. 1995, ApJ, 447, 364
Duffy, P., Drury, L. O., & Völk, H. J. 1994, A&A, 291, 613
Ellison, D. C., & Cassam-Chenaï, G. 2005, ApJ, 632, 920
Fahr, H. J., Kausch, T., & Scherer, H. 2000, A&A, 357, 268
Falle, S. A. E. G., & Giddings, J. R. 1987, MNRAS, 225, 399
Ferrière, K. 1998, ApJ, 497, 759
Frank, A., Jones, T. W., & Ryu, D. 1995, ApJ, 441, 629
Ghavamian, P., Laming, J. M., & Rakowski, C. E. 2007, ApJ, 654, L69
Ghavamian, P., Raymond, J. C., Hartigan, P., & Blair, W. P. 2000, ApJ, 535, 266
Ghavamian, P., Raymond, J. C., Smith, R. C., & Hartigan, P. 2001, ApJ, 547, 995
Ghavamian, P., Winkler, P. F., Raymond, J. C., & Long, K. S. 2002, ApJ, 572, 888
Gotthelf, E. V., Koralesky, B., Rudnick, L., Jones, T. W., Hwang, U., & Petre, R. 2001, ApJ, 552, L39
Heng, K., & McCray, R. 2007, ApJ, 654, 923
Heng, K., van Adelsberg, M., McCray, R., & Raymond, J. C. 2007, ApJ, 668, 275
Hester, J. J. 1987, ApJ, 314, 187
Hester, J. J., Raymond, J. C., & Blair, W. P. 1994, ApJ, 420, 721
Hwang, U., Decourchelle, A., Holt, S. S., & Petre, R. 2002, ApJ, 581, 1101
Jones, T. W., & Kang, H. 1990, ApJ, 363, 499
Jones, T. W., & Kang, H. 1992, ApJ, 396, 575
Jun, B. I., & Jones, T. W. 1997, ApJ, 481, 253
Kamper, K. W., & van den Bergh, S. 1978, ApJ, 224, 851
Kang, H., & Jones, T. W. 1990, ApJ, 353, 149
Kang, H., & Jones, T. W. 1995, ApJ, 447, 944
Kang, H., & Jones, T. W. 1997, ApJ, 476, 875
Kang, H., & Jones, T. W. 2006, Astropart. Phys., 25, 246
Kang, H., Jones, T. W., & Ryu, D. 1992, ApJ, 385, 193
Kirshner, R., Winkler, P. F., & Chevalier, R. A. 1987, ApJ, 315, L135
Ko, C.-M., Chan, K.-W., & Webb, G. M. 1997, J. Plasma Phys., 57, 677
Korreck, K. E. 2005, Ph.D. thesis, University of Michigan
Koyama, K., Petre, R., Gotthelf, E. V., Hwang, U., Matsuura, M., Ozaki, M., & Holt, S. S. 1995, Nature, 378, 255
Laming, J. M. 2001, ApJ, 546, 1149

Lee, J.-J., Koo, B.-C., Raymond, J. C., Ghavamian, P., Pyo, T.-S., Tajitsu, A., & Hayashi, M. 2007, ApJ, 659, L133
Lee, J.-J., Koo, B.-C., & Tatematsu, K. 2004, J. Korean Astron. Soc., 37, 223
Lim, A. J., & Raga, A. C. 1995, MNRAS, 277, 353
Long, K. S., Reynolds, S. P., Raymond, J. C., Winkler, P. F., Dyer, K. K., & Petre, R. 2003, ApJ, 586, 1162
MacKenzie, J. F., & Voelk, H. J. 1982, A&A, 116, 191
Malkov, M. A., & Diamond, P. H. 2006, ApJ, 642, 244
Malkov, M. A., Diamond, P. H., & Völk, H. J. 2000, ApJ, 533, L171
Markiewicz, W. J., Drury, L. O., & Völk, H. J. 1990, A&A, 236, 487
Michael, E., et al. 2003, ApJ, 593, 809
Mond, M., & Drury, L. O. 1998, A&A, 332, 385
Morfill, G. E., Aschenbach, B., & Drury, L. O. 1984, Nature, 311, 358
Niemiec, J., Pohl, M., Stroman, T., & Nishikawa, K. I. 2008, ApJ, 684, 1174
Parizot, E., Marcowith, A., Ballet, J., & Gallant, Y. A. 2006, A&A, 453, 387
Raymond, J. C. 2001, Space Sci. Rev., 99, 209
Raymond, J. C., Blair, W. P., Fesen, R. A., & Gull, T. R. 1983, ApJ, 275, 636
Raymond, J. C., Holman, G., Ciaravella, A., Panasyuk, A., Ko, Y.-K., & Kohl, J. 2007, ApJ, 659, 750
Raymond, J. C., Isenberg, P. A., & Laming, J. M. 2008, ApJ, 682, 408
Sankrit, R., Blair, W. P., Delaney, T., Rudnick, L., Harrus, I. M., & Ennis, J. A. 2005, Adv. Space Res., 35, 1027
Schwarz, U. J., Goss, W. M., Kalberla, P. M., & Benaglia, P. 1995, A&A, 299, 193
Smith, R. C., Kirshner, R. P., Blair, W. P., & Winkler, P. F. 1991, ApJ, 375, 652
Smith, R. C., Raymond, J. C., & Laming, J. M. 1994, ApJ, 420, 286
Sollerman, J., Ghavamian, P., Lundqvist, P., & Smith, R. C. 2003, A&A, 407, 249
Strom, R. G. 1988, MNRAS, 230, 331
Strong, A. W., Moskalenko, I. V., & Ptuskin, V. S. 2007, Annu. Rev. Nucl. Part. Sci., 57, 285
van Adelsberg, M., Heng, K., McCray, R., & Raymond, J. C. 2008, arXiv:0803.2521
Vink, J., & Laming, J. M. 2003, ApJ, 584, 758
Völk, H. J., Berezhko, E. G., & Ksenofontov, L. T. 2003, A&A, 409, 563
Völk, H. J., Berezhko, E. G., & Ksenofontov, L. T. 2005, A&A, 433, 229
Völk, H. J., Berezhko, E. G., & Ksenofontov, L. T. 2007, Ap&SS, 309, 389
Völk, H. J., Drury, L. O., & McKenzie, J. F. 1984, A&A, 130, 19
Völk, J. H., & McKenzie, F. J. 1981, International Cosmic Ray Conference, Vol. 9, ed. T. Montmerle (Saclay: Centre d'Études Nucleaires), 246
Wagner, A. Y., Falle, S. A. E. G., & Hartquist, T. W. 2007, A&A, 463, 195
Wagner, A. Y., Falle, S. A. E. G., Hartquist, T. W., & Pittard, J. M. 2006, A&A, 452, 763
Warren, J. S., et al. 2005, ApJ, 634, 376
Webb, G. M., Drury, L. O., & Völk, H. J. 1986, A&A, 160, 335
Whang, Y. C. 1997, ApJ, 485, 389
Zank, G. P., Webb, G. M., & Donohue, D. J. 1993, ApJ, 406, 67
Zirakashvili, V. N., Breitschwerdt, D., Ptuskin, V. S., & Völk, H. J. 1996, A&A, 311, 113
Zirakashvili, V. N., Ptuskin, V. S., & Völk, H. J. 2008, ApJ, 678, 255